AIP | Applied Physics Letters

Bi(Ni1/2Zr1/2)O3-PbTiO3 relaxor-ferroelectric films for piezoelectric energy harvesting and electrostatic storage

Zhenkun Xie, Zhenxing Yue, Griffin Ruehl, Bin Peng, Jie Zhang, Qi Yu, Xiaohua Zhang, and Longtu Li

Citation: Applied Physics Letters **104**, 243902 (2014); doi: 10.1063/1.4884427
View online: http://dx.doi.org/10.1063/1.4884427
View Table of Contents: http://scitation.aip.org/content/aip/journal/apl/104/24?ver=pdfcov
Published by the AIP Publishing

$Bi(Ni_{1/2}Zr_{1/2})O_3$-$PbTiO_3$ relaxor-ferroelectric films for piezoelectric energy harvesting and electrostatic storage

Zhenkun Xie,[1] Zhenxing Yue,[1,a)] Griffin Ruehl,[2] Bin Peng,[1] Jie Zhang,[1] Qi Yu,[1] Xiaohua Zhang,[1] and Longtu Li[1]
[1]*State Key Laboratory of New Ceramics and Fine Processing, School of Materials Science and Engineering, Tsinghua University, Beijing 100084, People's Republic of China*
[2]*Department of Chemical and Biological Engineering, Montana State University, Bozeman, Montana 59717, USA*

(Received 7 April 2014; accepted 9 June 2014; published online 17 June 2014)

In this Letter, we demonstrated that both a high energy-storage density and a large piezoelectric response can be attained simultaneously in relaxor-ferroelectric $0.4Bi(Ni_{1/2}Zr_{1/2})O_3$-$0.6PbTiO_3$ films prepared by chemical solution deposition. The as-prepared films had a pure-phase perovskite structure with an excellent crystalline morphology, featuring a moderate relative permittivity ($\varepsilon_r \sim 800$–1100), a low dissipation factor ($\tan\delta < 5\%$) and strong relaxor-like behavior ($\gamma = 1.81$). An ultra-high energy-storage density of 39.8 J/cm^3 at 2167 kV/cm was achieved at room temperature. Moreover, the $0.4Bi(Ni_{1/2}Zr_{1/2})O_3$-$0.6PbTiO_3$ films exhibited a considerably large effective piezoelectric coefficient of 83.1 pm/V under substrate clamping, which is comparable to the values obtained for lead zirconate titanate films. Good thermal stabilities in both the energy-storage performance and the piezoelectric properties were obtained over a wide range of temperatures, which makes $0.4Bi(Ni_{1/2}Zr_{1/2})O_3$-$0.6PbTiO_3$ films a promising candidate for high energy-storage embedded capacitors, piezoelectric micro-devices, and specifically for potential applications in next-generation integrated multifunctional piezoelectric energy harvesting and electrostatic storage systems. © *2014 AIP Publishing LLC*. [http://dx.doi.org/10.1063/1.4884427]

With the rapid development of microelectronics, micromachining technologies, and wireless sensing technologies, piezoelectric energy harvesting (PEH) from ambient vibrations or human motion has attracted considerable attention, because ambient mechanical vibration is ubiquitous and easily accessible through micro-electromechanical system (MEMS) technologies for energy conversion.[1–4] However, the major drawback encountered in PEH is that the average harvested power is too low to directly power most electronic circuits. Therefore, specific energy-storage devices are needed to store and accumulate the harvested energy for intermittent use. Most of the recent research on PEH employs rechargeable batteries or super-capacitors as the energy-storage devices, because of their high energy-storage density compared with conventional capacitors.[5,6] Nevertheless, with the development of electronic devices toward miniaturization, light weight, and integration, it is not convenient and easy to design and integrate rechargeable batteries or super-capacitors into PEH system. Although multifunctional self-charge structures have received much attentions in recent years,[7,8] designing the piezoelectric layer and the thin-film battery layer is still complicated. If a multifunctional piezoelectric film material that possesses both a large piezoelectric response and a high energy-storage density could be developed and used as the piezoelectric energy generator and energy-storage material, it will significantly simplify electronic circuits and make the integration and assembly of electronic devices much easier. Moreover, the technique of integrating functional electro-ceramic films into Si-based MEMS structures offers the ability to integrate large device arrays on a wafer and facilitates the development of next-generation integrated PEH systems.[9]

Generally, the energy-storage density (W) in dielectric capacitors is calculated according to the polarization-electric field hysteresis (P-E) loops with the formula

$$W = \int_{P_r}^{P_{max}} EdP,$$

where E is the applied field, P is the polarization, P_{max} is the maximum polarization, and P_r is the remanent polarization. It can be deduced from this formula that to obtain a higher W value, a larger maximum (with a lower remanent) polarization and a higher electric breakdown strength are required. Therefore, compared with the bulk ceramic counterparts, thin-film materials are more likely to exhibit better energy-storage performance, owing to their higher electric-field endurance. Unfortunately, the energy-storage density of conventional piezoelectric film materials, such as lead zirconate titanate (PZT), are small because of their relatively low electric breakdown field, even though they have excellent piezoelectric performance.[10] In the past few years, polymer-ferroelectric, anti-ferroelectric, and relaxor-ferroelectric films have shown better potential and higher energy-storage density than conventional linear dielectrics.[11–15] However, the piezoelectric properties in these polymer-ferroelectric and anti-ferroelectric films are poor, resulting in low piezoelectric conversion efficiencies.

Recently, bismuth-based solid solutions of $BiMeO_3$-$PbTiO_3$ (where Me is either a single cation or the combination of mixed cations with an average trivalence) have

a)Author to whom correspondence should be addressed. Electronic mail: yuezhx@mail.tsinghua.edu.cn

received ever-increasing interest, owing to their high polarization and large piezoelectric response at high temperatures.[16–21] The improved ferroelectric and piezoelectric performances are primarily due to the strong hybridization between the Pb/Bi(6*s*,6*p*) and O(2*p*) orbitals.[22,23] For instance, ultra-large piezoelectric coefficients (d_{33}) have been achieved in $BiScO_3$-$PbTiO_3$ ($d_{33} \sim 460$ pC/N)[16,17] and $Bi(Ni_{1/2}Hf_{1/2})O_3$-$PbTiO_3$ ($d_{33} \sim 446$ pC/N)[18] ceramics at their morphotropic phase boundary (MPB), which are even superior to the traditional PZT ceramics. But their potential applications in devices are restricted greatly because of the high cost of Sc and Hf. $xBi(Ni_{1/2}Zr_{1/2})O_3$–$(1-x)PbTiO_3$ is another bismuth-based solid solution with a comparably large piezoelectric response ($d_{33} \sim 400$ pC/N), low cost, and strong relaxor behavior for the MPB compositions ($x = 0.4$),[19] thus it is more likely to be a potential candidate for commercial applications in PEH systems. However, studies on $Bi(Ni_{1/2}Zr_{1/2})O_3$-$PbTiO_3$ solid solution films are still lacking. Hence, in this present work, the dielectric, ferroelectric, and piezoelectric properties as well as energy-storage performance of $0.4Bi(Ni_{1/2}Zr_{1/2})O_3$-$0.6PbTiO_3$ (0.4BNZ-0.6PT) films fabricated by chemical solution deposition (CSD) were investigated comprehensively. Interestingly, we have found that 0.4BNZ-0.6PT films exhibited a high energy-storage density and a large piezoelectric response simultaneously. Moreover, the energy-storage performance and piezoelectric behavior displayed good thermal stability over a wide range of operating temperatures.

The capacitors were fabricated on Pt(111)/Ti/SiO_2/Si substrates with 0.4BNZ-0.6PT films as the dielectric layer by CSD. $Pb(COOCH_3)_2{\cdot}3H_2O$, $Ti(OCH(CH_3)_2)_4$, $Bi(NO_3)_3{\cdot}5H_2O$, $Ni(COOCH_3)_2{\cdot}4H_2O$, and $Zr(OCH(CH_3)_2)_4$ were chosen as the raw materials for the precursor solutions together with glacial acetic acid, isopropyl alcohol, and distilled water as the solvent. Acetylacetone, 2-methoxyethanol, and methanamide were then added to avoid the appearance of cracks. A similar process of precursor solution was reported in our previous work.[24] The composition of the solution was controlled to yield $0.4Bi(Ni_{1/2}Zr_{1/2})O_3$–$0.6PbTiO_3$ with 5% excess Pb and Bi to compensate for volatilization and oxidation during the following repeated thermal processing. The resulting mixture was stirred continuously and subsequently deposited onto Pt(111)/Ti/SiO_2/Si substrates by spin-coating at 5000 rpm for 30 s, followed by pyrolysis at 500 °C for 5 min. The deposition-pyrolysis cycle was repeated until the desired film thickness was reached. Finally, the films were annealed at 700 °C for 5 min for crystallization.

The structure was examined by X-ray diffraction (XRD, D/max-2500, Rigaku; Japan) using Cu-Kα radiation. The morphologies of film surfaces and cross-sections were observed by atomic force microscopy (AFM) and field-emission scanning electron microscopy (SEM), respectively. The depth profiles of the films were obtained by Auger electron spectroscopy (AES, PHI 700, ULVAC-PHI, Japan) with Ar^+ ion sputtering at a sputter rate of 52 nm/min. The dielectric properties were investigated with an impedance analyzer (4294A, Agilent, CA, USA). A ferroelectric test module (TF-2000 Analyzer, axiACCT, Germany) was employed to evaluate the ferroelectric properties. The temperature was controlled with a temperature control system (THMS600, Guildford, U.K.). The local effective piezoelectric coefficients (d_{33}) for the films were characterized by a scanning probe microscopy (SPM, SPI4000&SPA300HV, Seiko, Japan) system with a conductive Rh-coated Si cantilever (SI-DF3) under the contact mode, which had a spring constant of 1.9 N/m and a free resonance frequency of 28 kHz.

The XRD pattern of the CSD-derived 0.4BNZ-0.6PT films indicates that the as-prepared films exhibit a pure-phase polycrystalline perovskite structure without any other secondary phases detected within the detection limit, as shown in Fig. 1(a). The surface topography was observed by

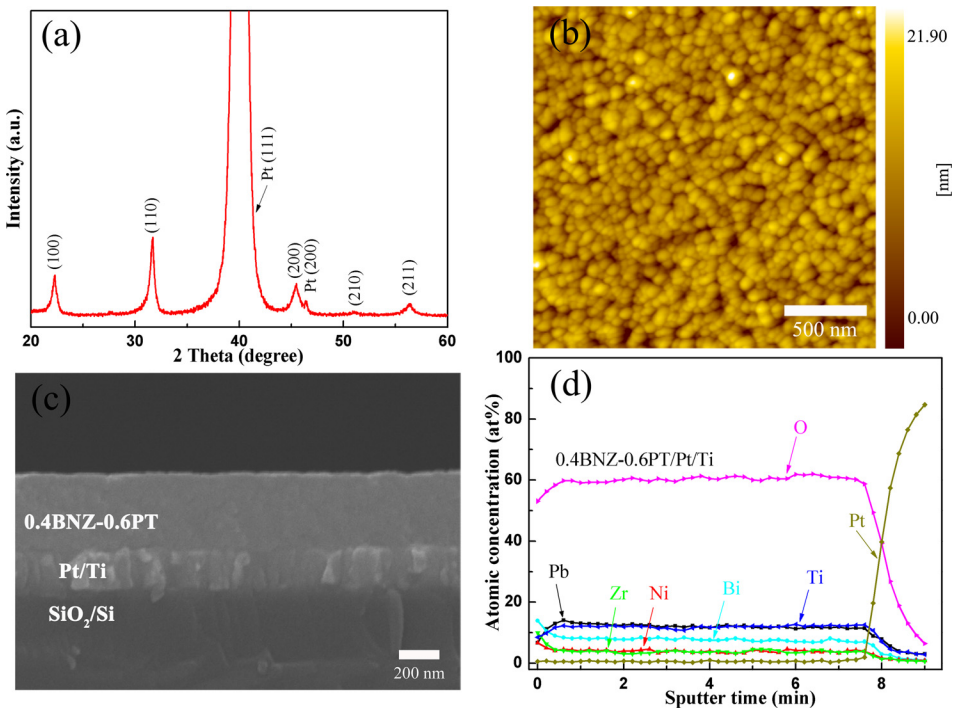

FIG. 1. (a) XRD pattern of 0.4BNZ-0.6PT films on Pt(111)/Ti/SiO_2/Si substrates. (b) Topography AFM image of the films. (c) Cross-section SEM image of the films. (d) AES depth profiles of the films.

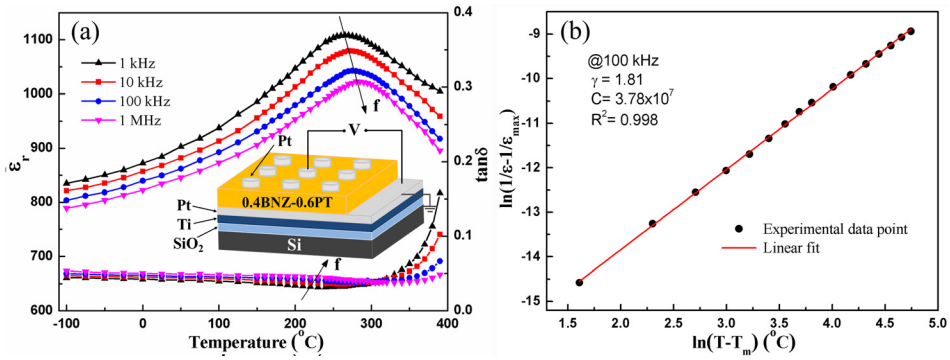

FIG. 2. (a) Temperature dependence of the dielectric behaviors in the 0.4BNZ-0.6PT films from 1 kHz to 1 MHz. Inset shows a schematic structure of set up for the electrical measurements. (b) $\ln(1/\varepsilon_r - 1/\varepsilon_{r,\max})$ as a function of $\ln(T - T_m)$ for the films. The symbols are experiment data, and the solid line is the fitting line.

AFM, as illustrated in Fig. 1(b), in which the 0.4BNZ-0.6PT films show uniform and granular feature with a measured roughness (RMS) of approximately 2.8 nm and an average grain size of ~55 nm. Cross-sectional SEM image of the 0.4BNZ-0.6PT films reveals that the films are well grown on Pt(111)/Ti/SiO_2/Si substrate without any cracks or pores, and the film thickness is about 400 nm, as shown in Fig. 1(c). The AES depth profiles of the samples confirm that the composition distribution along the thickness direction is homogeneous with a Pb/Bi ratio close to the predesigned value of 60/40 in the precursor solution; except for the superficial region and the transient layer close to the Pt electrodes, as shown in Fig. 1(d).

To measure the electrical properties, top platinum electrodes were sputtered on the films through a shadow mask with a diameter of 250 μm to form Pt/0.4BNZ-0.6PT/Pt capacitor structures, as shown in the inset of Fig. 2(a). The temperature-dependent dielectric behaviors of the films at different frequencies are presented in Fig. 2(a). The films exhibit a moderate relative permittivity ($\varepsilon_r \sim 800$–1100), and a low dissipation factor ($\tan\delta < 5\%$) over a large range of temperatures of -100 to 350 °C. This suggests that the 0.4BNZ-0.6PT films have the potential for capacitor applications in high-temperature conditions, such as automotive, aerospace, and other related industries. The broad relative permittivity peaks in the films, which are much broader than their counterparts in bulk form,[19] manifest a typical diffusive phase transition (DPT) corresponding to a ferroelectric-paraelectric phase transition. Moreover, the maximum permittivity ($\varepsilon_{r,\max}$) decreases with the increase of frequency, while the temperature of the maximum permittivity (T_m) shifts toward higher temperature side, indicative of typical relaxor-like behavior in the 0.4BNZ-0.6PT films. The diffuseness of the phase transition can be described by the modified Curie-Weiss law,[25] which can be expressed as $1/\varepsilon_r - 1/\varepsilon_{r,\max} = C^{-1}(T - T_m)^{\gamma}$, where C is a Curie-like constant and γ is the degree of diffuseness, which varies between 1 for a normal ferroelectric and 2 for an ideal relaxor ferroelectric. The plot of $\ln(1/\varepsilon_r - 1/\varepsilon_{r,\max})$ as a function of $\ln(T - T_m)$ at 100 kHz is displayed in Fig. 2(b). A good linear relationship is observed for the samples and the slope of the fitting curves γ is 1.81, suggesting that there is a large relaxation of the permittivity and relaxor-like behavior in 0.4BNZ-0.6PT films.

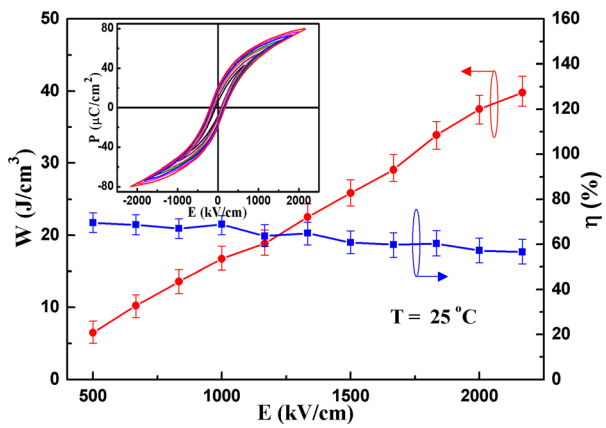

FIG. 3. Recoverable energy-storage density and efficiency as a function of applied field for the 0.4BNZ–0.6PT films at room temperature. The inset shows *P-E* loops (1 kHz) for the films under various electric fields at room temperature.

Room-temperature *P-E* loops of the 0.4BNZ-0.6PT films were measured under various electric fields at 1 kHz, as shown in the inset of Fig. 3. The films exhibit slim *P-E* loops at high electric fields, further demonstrating the relaxor behavior and high electric-field endurance of the films. The improved electric-field endurance of the films compared with the ceramic counterpart is mainly attributed to the uniform and pore-free microstructures as observed in Fig. 1. Figure 3 presents the external field-dependent recoverable energy-storage density (W) and efficiency (η) of the films at room temperature at 1 kHz. As expected, the W value is enhanced almost linearly with the increase of applied field, whilst the value of η shows a contrary tendency. A maximum W value of 39.8 J/cm^3 and a high η value of 56.5% are obtained under an electric field of 2167 kV/cm. Specifically, the energy-storage density obtained in the 0.4BNZ-0.6PT films is much larger than that of the traditional PZT piezoelectric films,[10] and is commensurate even with the high-end value reported for polymer-ferroelectric and antiferroelectric films.[11–14] Thus, it can be concluded that the 0.4BNZ-0.6PT film could be a promising candidate for applications in high energy-storage density capacitors.

It is known that high-temperature stability is essential in the application of dielectric capacitors. Figure 4 depicts the temperature-dependent *P-E* loops for the 0.4BNZ-0.6PT films measured in the temperature range of -100 to 200 °C at 1500 kV/cm. As shown in Fig. 4, the shape of the hysteresis loops strongly depends on the temperature, and the loops become slimmer at high temperatures. With the rise of temperature, the values of $P_{\max}$, P_r, and the coercive field (E_c) all diminishes, whilst the back-switching polarization

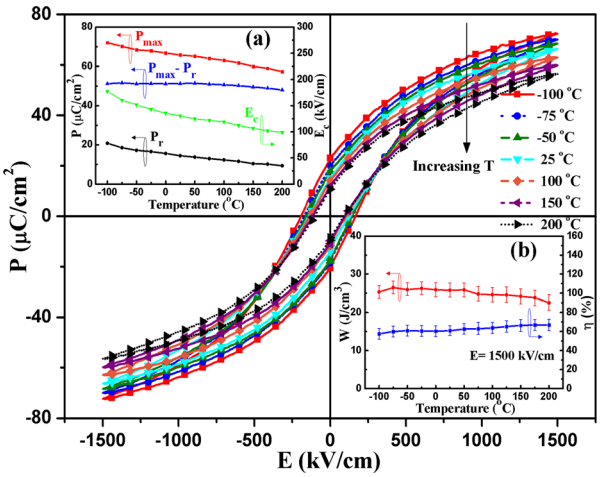

FIG. 4. Temperature-dependent *P-E* loops of 0.4BNZ-0.6PT films measured at 1500 kV/cm. The inset shows corresponding P_{max}, P_r, P_{max}-P_r, and E_c values (a), and energy-storage density and efficiency (b) under various temperatures.

(P_{max}–P_r) almost maintains the same value, varying slightly from 51.2 to 48.1 μC/cm^2, as evidenced in the inset (a) of Fig. 4. Because of the small variation in the P_{max}–P_r values, the calculated W values slightly fluctuate between 25.4 and 22.5 J/cm^3, and the η values remain at around 60% under 1500 kV/cm, as shown in the inset (b) of Fig. 4. These results demonstrate the excellent temperature stability of 0.4BNZ-0.6PT films for energy-storage within the temperature range measured, which could be attributed to the broad DPT behavior, as observed in Fig. 2.

Simultaneously, the piezoelectric properties of the 0.4BNZ-0.6PT films were characterized with a SPM system. The measurements of the local piezoelectric displacement were carried out at piezoelectric force microscopy (PFM) mode by keeping the SPM tip in contact with the surface of the samples and applying a DC voltage from −10 to 10 V to record the piezo-response signal.[26–28] As shown in the inset (a) of Fig. 5, a typical butterfly-shaped piezoresponse loop is observed with a maximum displacement of 0.77 nm at −9.5 V and at room temperature. The effective piezoelectric

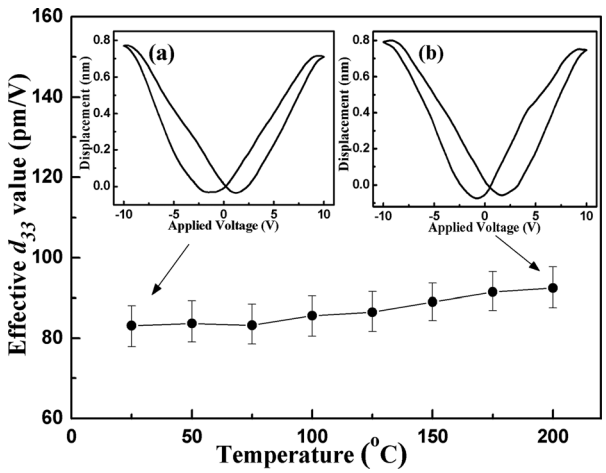

FIG. 5. Temperature dependence of effective d_{33}^* for the 0.4BNZ-0.6PT films, the insets show the measured local piezoelectric response dependence of the applied voltage at 25 °C and 200 °C, respectively.

coefficient d_{33} is estimated to be approximately 83.1 pm/V. The observed piezoelectric coefficients in the 0.4BNZ-0.6PT films are much lower than that of their counterparts because of the clamping effect imposed by the substrates.[19] However, the d_{33} values of the films are comparable to the values obtained for the traditional PZT films (~80 pm/V).[28] More importantly, the piezoelectric properties of the 0.4BNZ-0.6PT films could be further enhanced by controlling the orientation, i.e., textured or epitaxial control.[29] Furthermore, the temperature dependence of d_{33} for the films was also measured by SPM under a high vacuum (1.0×10^{-4} Pa), as shown in Fig. 5. As the temperature increases, the d_{33} only changes slightly from 83.1 pm/V at 25 °C to 92.4 pm/V at 200 °C, indicating that the piezoelectric properties in the 0.4BNZ-0.6PT films were not temperature sensitive. The slight increase may be ascribed to the less-constrained state of the motion of domains at higher temperatures. The stable and good piezoelectric properties over a broad temperature range indicate that the 0.4BNZ-0.6PT films are good candidates for applications in high-performance MEMS devices. In general, it seems very hard to find materials to be appropriate for both PEH and energy storage simultaneously, because all PEH figures of merits (FoM) are inversely proportional to the value of relative permittivity, while energy-storage devices often utilize high dielectric materials. However, as the energy harvesting FoM is proportional to the square of piezoelectric coefficient, the large piezoelectric response, moderate permittivity and high energy-storage density with good temperature stabilities make the relaxor-ferroelectric 0.4BNZ-0.6PT films a potential solution for the development of next-generation, integrated, multifunctional PEH, and electrostatic storage systems. Additionally, its application will be further developed if the permittivity and piezoelectric coefficient could be properly optimized in future research.

In summary, relaxor-ferroelectric 0.4BNZ-0.6PT films with pure perovskite structure as well as dense and uniform microstructure were deposited on platinized silicon substrates by CSD. The films showed a moderate relative permittivity ($\varepsilon_r \sim 800$–1100), a low dissipation factor ($\tan\delta < 5\%$), and strong relaxor-like behavior ($\gamma = 1.81$) over a broad temperature range of −100 to 350 °C. The recoverable energy-storage density was enlarged with the increase of applied field, and an ultra-high energy-storage density of 39.8 J/cm^3 at 2167 kV/cm was achieved at room temperature. The clamped d_{33}^* was up to 83.1 pm/V, which could be comparable to conventional PZT films. Moreover, both the energy-storage performance and piezoelectric property exhibited good temperature stability. These excellent features indicate that the relaxor-ferroelectric 0.4BNZ-0.6PT films are promising candidates for applications in advanced capacitors with high energy-storage, high-performance MEMS devices and, in particular, they have potential for applications in the next-generation, integrated, multifunctional PEH, and electrostatic storage systems.

This work was financially supported by the Ministry of Science and Technology of China through 973-Project under No. 2009CB623306, and the Natural Science Foundation of China (Grant Nos. 51221291 and 51272125).

[1]C. R. Bowen, H. A. Kim, P. M. Weaver, and S. Dunn, Energy Environ. Sci. **7**, 25 (2014).
[2]Y. B. Jeon, R. Sood, J. H. Jeong, and S. G. Kim, Sens. Actuators, A **122**, 16 (2005).
[3]J. M. Donelan, Q. Li, V. Naing, J. A. Hoffer, D. J. Weber, and A. D. Kuo, Science **319**, 807 (2008).
[4]C. Yeagera and S. Trolier-McKinstry, J. Appl. Phys. **112**, 074107 (2012).
[5]H. A. Sodano, D. J. Inman, and G. Park, J. Intell. Mater. Syst. Struct. **16**, 799 (2005).
[6]M. J. Guan and W. H. Liao, J. Intell. Mater. Syst. Struct. **19**, 671 (2008).
[7]S. R. Anton, A. Erturk, and D. J. Inman, Smart Mater. Struct. **19**, 115021 (2010).
[8]S. R. Anton, A. Erturk, and D. J. Inman, J. Aircr. **49**, 292 (2012).
[9]N. Setter, *Electroceramic-Based MEMS Fabrication-Technology and Applications* (Springer Science, New York, 2005).
[10]J. Sigman, G. L. Brennecka, P. G. Clem, and B. A. Tuttle, J. Am. Ceram. Soc. **91**, 1851 (2008).
[11]B. J. Chu, X. Zhou, K. Ren, B. Neese, M. Lin, Q. Wang, F. Bauer, and Q. M. Zhang, Science **313**, 334 (2006).
[12]M. Rahimabady, L. Q. Xu, S. Arabnejad, K. Yao, L. Lu, V. W. Shim, K. G. Neoh, and E. T. Kang, Appl. Phys. Lett. **103**, 262904 (2013).
[13]X. H. Hao, J. W. Zhai, L. B. Kong, and Z. K. Xu, Prog. Mater. Sci. **63**, 1 (2014).
[14]X. H. Hao, J. W. Zhai, and X. Yao, J. Am. Ceram. Soc. **92**, 1133 (2009).
[15]S. Tong, B. H. Ma, M. Narayanan, S. S. Liu, R. Koritala, U. Balachandran, and D. L. Shi, ACS Appl. Mater. Interface **5**, 1474 (2013).
[16]R. E. Eitel, C. A. Randall, T. R. Shrout, P. W. Rehrig, W. Hackenberger, and S. E. Park, Jpn. J. Appl. Phys., Part 1 **40**, 5999 (2001).
[17]R. E. Eitel, C. A. Randall, T. R. Shrout, and S. E. Park, Jpn. J. Appl. Phys. Part 1 **41**, 2099 (2002).
[18]Z. Pan, J. Chen, L. L. Fan, L. J. Liu, L. Fang, and X. R. Xing, J. Appl. Phys. **112**, 114120 (2012).
[19]Y. C. Rong, J. Chen, H. J. Kang, L. J. Liu, L. Fang, L. L. Fan, Z. Pan, and X. R. Xing, J. Am. Ceram. Soc. **96**, 1035 (2013).
[20]C. F. Zhong, L. M. Guo, X. H. Wang, and L. T. Li, J. Am. Ceram. Soc. **95**, 473 (2012).
[21]S. W. Ko, H. G. Yeo, and S. Trolier-Mckinstry, Appl. Phys. Lett. **95**, 162901 (2009).
[22]I. Grinberg, M. R. Suchomel, P. K. Davies, and A. M. Rappe, J. Appl. Phys. **98**, 094111 (2005).
[23]M. Yashima, K. Omoto, J. Chen, H. Kato, and X. R. Xing, Chem. Mater. **23**, 3135 (2011).
[24]Z. K. Xie, B. Peng, S. Q. Meng, Y. Y. Zhou, and Z. X. Yue, J. Am. Ceram. Soc. **96**, 2061 (2013).
[25]Z.-Y. Cheng, L.-Y. Zhang, and X. Yao, J. Appl. Phys. **79**, 8615 (1996).
[26]H. Wen, X. H. Wang, X. Y. Deng, and L. T. Li, Appl. Phys. Lett. **88**, 222904 (2006).
[27]L. X. Zhang, J. Chen, H. Q. Zhao, L. L. Fan, Y. C. Rong, J. X. Deng, R. B. Yu, and X. R. Xing, Appl. Phys. Lett. **103**, 082902 (2013).
[28]W. Gong, J. F. Li, X. C. Chu, Z. L. Gui, and L. T. Li, Acta Mater. **52**, 2787 (2004).
[29]R. Ramesh and D. G. Schlom, Science **296**, 1975 (2002).